

# Tunable quantum interference using a topological source of indistinguishable photon pairs

Venkata Vikram Orre,<sup>1,2,\*</sup> Sunil Mittal,<sup>1,2,†</sup> Elizabeth A. Goldschmidt,<sup>3</sup> and Mohammad Hafezi<sup>1,2,4</sup>

<sup>1</sup>*Joint Quantum Institute, NIST/University of Maryland, College Park, Maryland 20742, USA*

<sup>2</sup>*Department of Electrical and Computer Engineering and IREAP,  
University of Maryland, College Park, Maryland 20742, USA*

<sup>3</sup>*Department of Physics, University of Illinois at Urbana-Champaign, Urbana, Illinois 61801, USA*

<sup>4</sup>*Department of Physics, University of Maryland, College Park, MD 20742, USA*

Sources of quantum light, in particular correlated photon pairs that are indistinguishable in all degrees of freedom, are the fundamental resource that enables continuous-variable quantum computation and paradigms such as Gaussian boson sampling. Nanophotonic systems offer a scalable platform for implementing sources of indistinguishable photon pairs. However, such sources have so far relied on the use of a single component, such as a single waveguide or a ring resonator, which offers limited ability to tune the spectral and temporal correlations between photons. Here, we demonstrate the use of a topological photonic system comprising a two-dimensional array of ring resonators to generate indistinguishable photon pairs with dynamically tunable spectral and temporal correlations. Specifically, we realize dual-pump spontaneous four-wave mixing in this array of silicon ring resonators that exhibits topological edge states. We show that the linear dispersion of the edge states over a broad bandwidth allows us to tune the correlations, and therefore, quantum interference between photons by simply tuning the two pump frequencies in the edge band. Furthermore, we demonstrate energy-time entanglement between generated photons and show that our topological source is inherently protected against fabrication disorders. Our results pave the way for scalable and tunable sources of squeezed light that are indispensable for quantum information processing using continuous variables.

Spurred by the possibility of realizing continuous-variable quantum computation, and Gaussian boson sampling that holds near-term promise for quantum simulations and various graph-theory problems, nanophotonics systems have emerged as a natural platform to generate indistinguishable photon pairs and, in the strong nonlinearity regime, single-mode squeezed light [1–8]. Most on-chip sources of indistinguishable photon pairs have relied on dual-pump spontaneous four-wave mixing (DP-SFWM), a third-order nonlinear process, in silicon or silicon-nitride waveguides and ring resonators [4–8]. In this process, two pump photons at different frequencies annihilate and create two frequency-degenerate photons, called signal and idler. The tight mode confinement in nanophotonic waveguides and the use of a ring resonator has remarkably enhanced the strength of SFWM interactions, leading to enhanced pair generation rates and eventually on-chip sources of squeezed light [6–9]. Extensions of these simple single-element systems to multi-mode, multi-resonator systems can allow tunability and multiplexing of various spectral or temporal modes, and thereby, enable a significant reduction in physical resources [2, 10–12]. However, such extensions have so far remained elusive.

At the same time, the influx of ideas derived from the physics of topological insulators has led to a new paradigm of complex photonic devices that use arrays of coupled waveguides or resonators to achieve unprecedented control over the flow of photons [13–21]. More specifically, edge states, the hallmark of topological systems, exhibit unique features such as unidirectional (or helical) flow of photons confined to the boundaries of a system, linear dispersion, and an inherent robustness against disorders. Photonic edge states have now been used to realize robust optical delay lines [18, 20, 22], lasers [23–25], optical fibers [26], and reconfigurable pathways on chips [27, 28]. More recently, topological edge states

have been exploited in quantum photonic devices, to realize chiral quantum-optic interfaces between quantum dots and photonic crystals [29], topological beam-splitters for quantum interference of photons [30], and also topological sources of quantum light [31, 32]. In particular, in ref.[31] we implemented a topological source of distinguishable photon pairs using single-pump SFWM in a two-dimensional (2D) lattice of coupled ring resonators. Therefore, it is intriguing to investigate topologically-inspired photonic designs to develop tunable and robust sources of indistinguishable photon pairs.

In this article, we report the generation of indistinguishable photon pairs via dual-pump SFWM in a 2D lattice of coupled ring resonators. This lattice realizes the anomalous quantum Hall model for photons and exhibits topological edge states [20, 33–35]. We show that the linear dispersion of the edge states results in phase-matched generation of photon pairs throughout the edge band, and therefore, allow us to tune the spectral-temporal bandwidth of photon pairs by tuning the input pump frequencies in the edge band. To show that the generated photon pairs are indeed indistinguishable, we use the fact that our systems is time-reversal symmetric and therefore, supports two pseudo-spins that circulate around the lattice in opposite directions (Fig.1). We use these counter-propagating edge states to realize a Sagnac interferometer and deterministically split the indistinguishable photon pairs [5, 6, 36]. We then demonstrate Hong-Ou-Mandel (HOM) interference between split photons which unequivocally establishes their indistinguishability. Furthermore, we show that the tunability of the spectral bandwidth of our source manifests in the temporal width of the HOM interference dip. Finally, we demonstrate that the generated photon pairs are energy-time entangled [37] as expected for a SFWM process with a continuous-wave pump, and our source is robust against fabrication disorders. Our results could lead to the realization of on-chip, topolog-

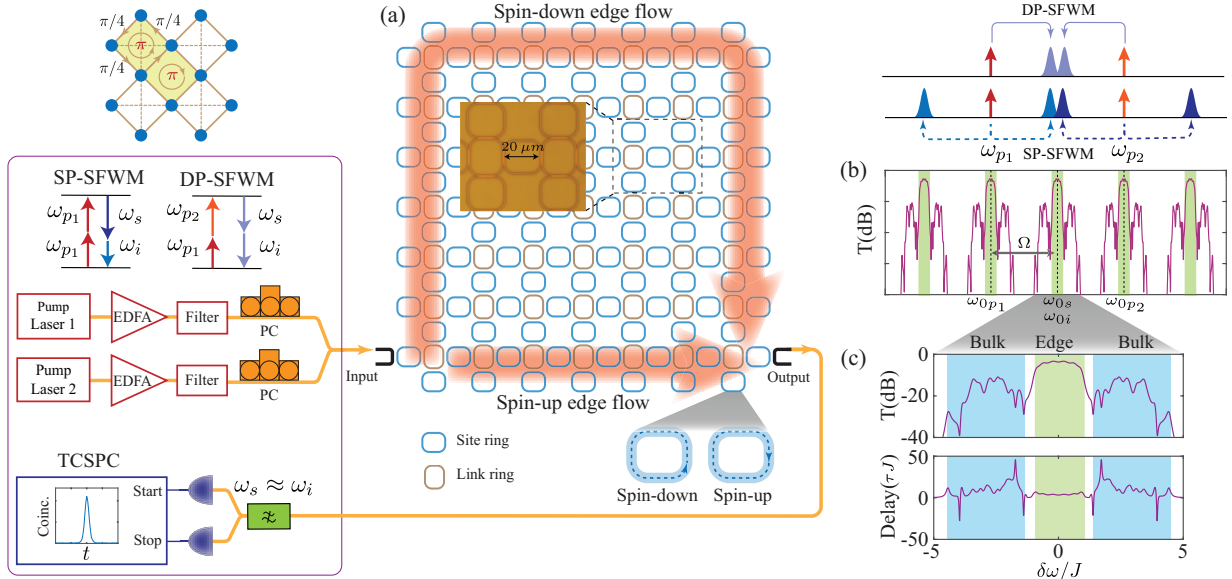


FIG. 1. (a) Schematic of the 2D array of silicon ring resonators that simulates the anomalous quantum-hall effect for photons. The link rings (shaded brown) couple nearest and next-nearest neighbor site rings (shaded blue), with hopping phases as shown in the inset. The lattice supports two pseudospins (up and down), with corresponding edge states travelling in opposite directions. (b,c) Simulated transmission and delay spectrum of the device showing edge and bulk bands. The spectra repeats after every FSR. To generate indistinguishable photon pairs via dual-pump SFWM, the lattice is pumped using two continuous-wave lasers, in different FSRs centered at  $\omega_{0p_1}$ , and  $\omega_{0p_1}$  (right inset). At the output, we use tunable filters, superconducting nanowire detectors (SNSPDs), and a time-interval analyzer to detect generated photon pairs, in the FSR centered at  $\omega_{s,i}$ , via time-resolved correlation measurements. This coincidence detection setup allows us to exclude frequency non-degenerate photons created by single pump SFWM (right inset). EDFA: erbium-doped fiber amplifier; PC: polarization controller; TCSPC:time-correlated single photon counter.

ically robust, and spectrally engineered sources of squeezed light for applications in continuous-variable quantum computation and gaussian boson sampling [1–3].

Our system consists of 2D checkerboard lattice of ring resonators (Fig.1a) [34, 35]. The rings (shaded blue) at the lattice sites are coupled to their nearest and next-nearest neighbors using another set of rings, which we call the link rings [18, 20]. The gap between the link and the site rings sets the strength ( $J$ ) of the evanescent field coupling between the site rings and is the same for both the nearest and next-nearest neighbor site rings. The resonance frequencies of the link rings are detuned from those of the site rings such that the link rings act as waveguides connecting site rings. More importantly, depending on their position, the link rings introduce a direction dependent hopping phase between the site rings. In our system, the link rings are positioned such that the hopping phases between next-nearest neighbor site rings is always zero, and that between nearest neighbor site rings is  $\pm\pi/4$ . This configuration effectively leads to the realization of a staggered synthetic magnetic field for photons such that the average magnetic flux through a unit cell of two plaquettes of the lattice is zero (shaded yellow in Fig.1a), but the flux through a single plaquette is non-zero. This coupled ring resonator configuration simulates the anomalous quantum Hall effect for photons [34, 35], with a Haldane-like tight-binding

Hamiltonian

$$H_L = \sum_{i,j} \omega_0 a_i^\dagger a_i - J \left( \sum_{\langle i,j \rangle} a_j^\dagger a_i e^{-i\phi_{i,j}} + \sum_{\langle\langle i,j \rangle\rangle} a_j^\dagger a_i + \text{h.c.} \right) \quad (1)$$

Here  $a_i^\dagger$  ( $a_i$ ) is the creation (annihilation) operator at a lattice site  $i = (x, y)$ . The summations  $\langle i, j \rangle$  and  $\langle\langle i, j \rangle\rangle$  are over the nearest and the next-nearest neighbor lattice sites, respectively.  $J$  is the coupling strength between the lattice sites, and is the same for both nearest and next nearest neighbors. The hopping phase  $\phi_{i,j} = \pm\pi/4$  for nearest-neighbor couplings and is zero for next-nearest neighbor couplings. The energy-momentum band structure of the lattice exhibits two bulk bands separated by a bandgap. For a finite lattice, the band gap hosts topological edge states that are confined to the boundary of the lattice. More importantly, the edge states are robust against disorders, such as, a mismatch in the ring resonance frequencies. Furthermore, they exhibit a linear dispersion [22, 34, 35]. The band structure of the lattice and the presence of edge states can be probed by measuring the transmission and the delay spectra of the lattice from input to the output port. The simulated transmission and delay spectra for a  $8 \times 8$  lattice are shown in Figs.1(b,c). The linear dispersion of the edge states manifests in the Wigner delay spectrum as a flat profile (Fig.1c) in the range  $\delta\omega = [-1, 1]J$ ,

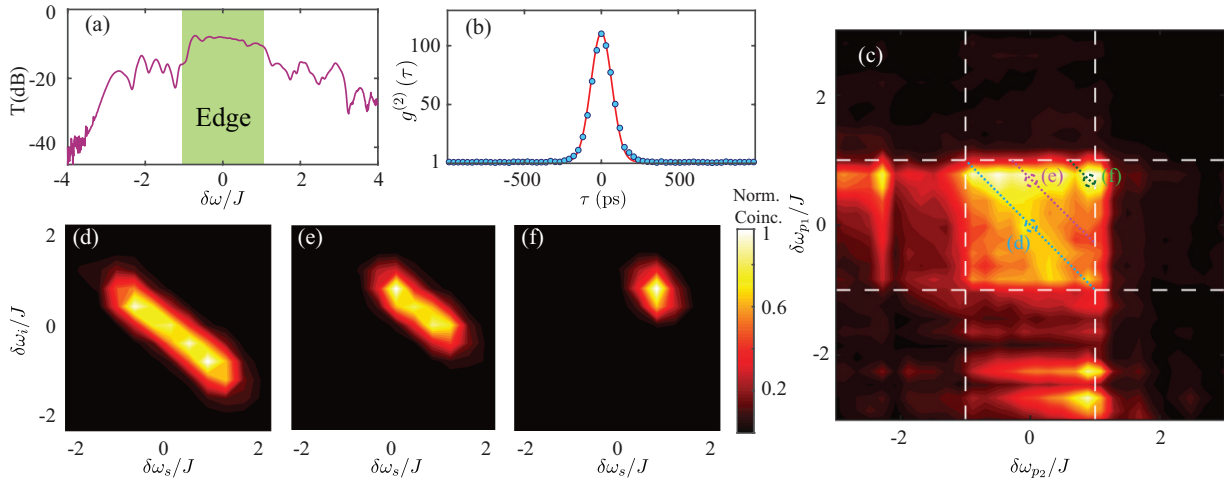


FIG. 2. (a) Measured transmission spectrum of an anomalous Hall device, with the edge band highlighted in green. (b) Measured second-order temporal correlation function  $g_2(\tau)$  showing that the photons are strongly correlated. (c) Measured coincidence counts as function of the input pump frequency detunings  $\delta\omega_{p1}, \delta\omega_{p2}$  relative to the respective longitudinal resonances. (d-f) Measured joint spectral intensity of the signal/idler photons, for input pump frequencies  $(\delta\omega_{p1}, \delta\omega_{p2}) = (0, 0)$ ,  $(0.8, 0)$   $J$ , and  $(0.8, 0.8)$   $J$ . The pump frequencies are also indicated in (c). The dashed lines show the spectra of generated photons in the edge band allowed by energy conservation.

where  $\delta\omega = \omega - \omega_0$  is the detuning of the excitation laser frequency ( $\omega$ ) from the ring resonance frequency ( $\omega_0$ ), for a given longitudinal mode. In contrast, the Wigner delay in the bulk band varies significantly because in a finite lattice, the bulk bands do not have a well defined momentum. Our system also supports a pseudospin degree of freedom because of the two circulation directions (clockwise and counter-clockwise) in the ring resonators. The two pseudospins (up and down) are time-reversed partners, and therefore, experience opposite hopping phases and exhibit counter propagating edge states [35].

Our devices are fabricated using the CMOS compatible silicon-on-insulator (SOI) platform at a commercial foundry (IMEC Belgium). The ring waveguides are  $\approx 510$  nm wide,  $\approx 220$  nm high, and at telecom wavelengths ( $\approx 1550$  nm), support a single TE polarized mode. The ring length is  $\approx 70\mu\text{m}$  with a free-spectral range of  $\approx 1$  THz. The coupling gap between the rings is 0.180 nm, and it results in a coupling strength  $J \simeq (2\pi)15.6$  GHz. The lattice is coupled to input and output waveguides as shown in Fig.1. At the ends of the input/output waveguides, we use grating couplers to inject light from standard single-mode fiber into the waveguides. Figure 2a shows the measured transmission spectrum of the device for spin-up excitation, with the edge band highlighted in color. The edge states for this excitation take the shorter route from input to the output coupler, as shown in Fig.1a.

To generate indistinguishable photon pairs in this lattice, we use the  $\chi^{(3)}$  nonlinearity of silicon and implement a dual-pump (DP) SFWM process. We pump the lattice using two classical, continuous-wave pump beams, at frequencies  $\omega_{p1}$  and  $\omega_{p2}$ . The DP-SFWM then leads to the generation of indistinguishable photon pairs, called signal and idler, at fre-

quencies  $\omega_s$  and  $\omega_i$ , respectively, such that the energy conservation relation  $\omega_{p1} + \omega_{p2} = \omega_s + \omega_i$  is satisfied. The pump frequencies are in fact positioned in two different longitudinal modes of the lattice separated by two free-spectral ranges (FSR,  $\Omega$ , see Fig.1). The indistinguishable photon pairs are then generated in the longitudinal mode located midway between the two pump modes, that is,  $\omega_{0p1} + \omega_{0p2} = \omega_{0s} + \omega_{0i}$  and  $\omega_{0s} = \omega_{0i}$ . Here  $\omega_{0\mu}$ , with  $\mu = p_1, p_2, s, i$ , is the resonance frequency of the respective longitudinal mode. This nonlinear process is described by the Hamiltonian

$$H_{\text{NL}} = \eta \sum_m \left( a_{m,s}^\dagger a_{m,i}^\dagger a_{m,p_1} a_{m,p_2} + a_{m,p_1}^\dagger a_{m,p_2}^\dagger a_{m,s} a_{m,i} \right). \quad (2)$$

Here  $\eta$  is the efficiency of the SFWM process, and  $a_{m,\mu}^\dagger$  is the photon creation operator for signal, idler or pump photons at a lattice site  $m$ . The DP-SFWM adds or removes photons in pairs, and therefore, in the low-loss regime, leads to single-mode squeezed light. We note that each of the two pump beams also generate distinguishable photon pairs via non-degenerate (single pump) SFWM (SP-SFWM). However, because of the energy conservation, these photon pairs are generated in longitudinal modes located symmetrically around the respective pump beams (Fig.1). Therefore, we use spectral filtering and time-resolved coincidence measurements between detected photon pairs to exclude the noise photons generated by single pump SFWM.

To understand the nature of spectral correlations between the two pump fields and the generated photons, we first measure the number of indistinguishable photon pairs generated via DP-SFWM as a function of the two pump frequency detunings ( $\delta\omega_{p1,2} = \omega_{p1,2} - \omega_{0p1,2}$ ), relative to their respective longitudinal mode center frequencies. As mentioned earlier,

we use time-resolved correlation measurements ( $g^{(2)}(\tau)$ ) to post-select the photon pairs generated by DP-SFWM. Figure 2b shows the typical temporal correlation function with pump powers  $P_1 = 1$  mW and  $P_2 = 3$  mW at the input of the lattice. We measure a maximum  $g^{(2)}(0) \simeq 117$  which shows that the two photons are indeed correlated. We integrate over the correlation peak to get the total number of coincidence counts in a given acquisition time (here 10 seconds). Figure 2c shows the measured number of coincidence counts as a function of the frequency detunings  $\delta\omega_{p_1}, \delta\omega_{p_2}$ . We observe that the photon generation rate is maximum when both the pump frequencies are in the edge band, that is, when  $\delta\omega_{p_1}, \delta\omega_{p_2} = [-1, 1]J$ . Furthermore, compared to the bulk band regions, the generation rate is relatively uniform throughout the edge band. We note that for a given choice of the two pump frequencies, energy and momentum conservation lead to spectral correlations between generated photons. However, our measurement of the number of generated photon pairs as a function of the pump frequencies does not resolve these spectral correlations.

To measure the spectral correlations between generated photons we fix the input pump frequencies to be in the middle of the edge band, at  $\delta\omega_{p_1} \simeq 0 \simeq \delta\omega_{p_2}$  and measure the spectral correlations between generated signal and idler photons [ $\Gamma(\delta\omega_s, \delta\omega_i)$ ], where  $\delta\omega_{s,i}$  are the frequency detunings of the signal or idler photons relative to their longitudinal mode resonances. The measured correlations show that, with the two pump fields in the edge band, the spectrum of generated signal and idler photons is also limited to the edge band. This is because of the linear dispersion of the edge states that leads to efficient phase matching (momentum conservation) when all the four fields are in the edge band, and also because of the confinement of the edge states to the lattice boundary that leads to a good spatial overlap between the fields. Furthermore, both the signal and idler spectra are centered around  $\delta\omega_s \simeq 0 \simeq \delta\omega_i$  which indicates that they are degenerate in frequency. Given the fact that our ring resonator waveguides support a single TE polarized mode and the generated photons are collected from a single spatial mode (the same output port), the generated photons are indistinguishable in all degrees of freedom. Note that we use continuous-wave pumps in our experiments, and the apparent width of spectral correlations along the diagonal is because of the finite spectral resolution ( $\approx 10$  GHz  $\simeq 0.64J$ ) of our measurements.

The energy conservation and the linear dispersion of the edge states also allows us to tune the spectral bandwidth of generated photons by tuning the input pump frequencies within the edge band region. This is because of the efficient momentum conservation in the edge band that limits the spectra of generated photons also to the edge band region. To show such tunability of the spectra of generated photons, we measure the signal-idler spectral correlations for different pump frequencies in the edge band. When both the pump frequencies are near the side of the edge band ( $\simeq 0.8J$ ), we observe that the spectra of generated photons are significantly narrower (by  $\approx 3X$ ) than that when both the pumps are in the center of the edge band (Fig.2). Also, as expected, the

spectra are centered around  $0.8J$ . Similarly, when the two pump frequencies are at different locations in the edge band ( $\delta\omega_{p_1} \simeq 0.8J, \delta\omega_{p_2} \simeq 0$ ), we observe that the spectra of generated photons are centered around  $0.4J$ , with a bandwidth larger than that with both the pumps in the side of the edge band.

Though our spectral measurements suggest that the generated photons are indistinguishable, Hong-Ou-Mandel (HOM) interference [38] can unambiguously confirm the indistinguishability of photons. In HOM interference, two indistinguishable photons arriving simultaneously at the two input ports of a beam-splitter bunch together at the output. However, in our topological source, both the photons are in a single spatial mode, they are degenerate in frequency, and have the same polarization. Therefore, as required for HOM interference, they can not be separated into two spatial modes using a normal beam-splitter which is probabilistic. Nevertheless, the two photons can be deterministically separated using time-reversed HOM interference at a beam-splitter when the input is a path-entangled state of the form  $|20\rangle_{A,B} + |02\rangle_{A,B}$ , that is, both the photons arrive either at the input port A or at port B of the beamsplitter. Here the state  $|nm\rangle_{A,B}$  refers to  $n$  photons in the first port of the beamsplitter and  $m$  photons in the second port.

To implement this deterministic beamsplitter, we use our topological source in a Sagnac interferometer (formed by beamsplitter BS-1, Fig.3a) [6, 36]. In this configuration, both the pseudospins (up and down) associated with our source are simultaneously pumped. Because they are time-reversed partners, the pump beams corresponding to the two pseudospins propagate through the same edge state, but in opposite directions, and generate an entangled two-photon state  $|20\rangle_{A,B} + e^{i\delta}|02\rangle_{A,B}$  at ports A, B of the beamsplitter BS-1. We note that the strength of SFWM interaction in our experiment is very weak such that the probability of generating two photon pairs, one in each arm of the Sagnac interferometer, is small. The relative phase  $\delta$  of two-photon entangled state can be set to 0 or  $\pi$  by appropriately choosing the input ports for the two pump beams at the Sagnac beamsplitter (BS 1 in Fig.3a) [6]. When both the pumps are in the same port of the BS-1 (Port C or Port D), the phase  $\delta = \pi$ , and the two photons bunch at the output of BS-1, that is, they appear at either port C or port D of BS-1 (Fig.3). In contrast, when the two pumps are in different ports of the beamsplitter BS-1 (one in Port C, and the other in Port D), the phase  $\delta = 0$  and it leads to anti-bunching of photons such that the photons are deterministically separated at the output of the BS-1. In our experiment, we use two circulators to collect the photons at ports C and D. For  $\delta = 0$ , we measure the probability of anti-bunching to be 0.89(1), and for  $\delta = \pi$ , we measure the total probability of bunching (in either port C or port D) to be 0.86(1). We emphasize that the use of a Sagnac interferometer, with the two pump beams injected at different input ports, alleviates the need for any active stabilization of our source.

To demonstrate HOM interference we set  $\delta = 0$  such that the two photons are deterministically separated in the ports

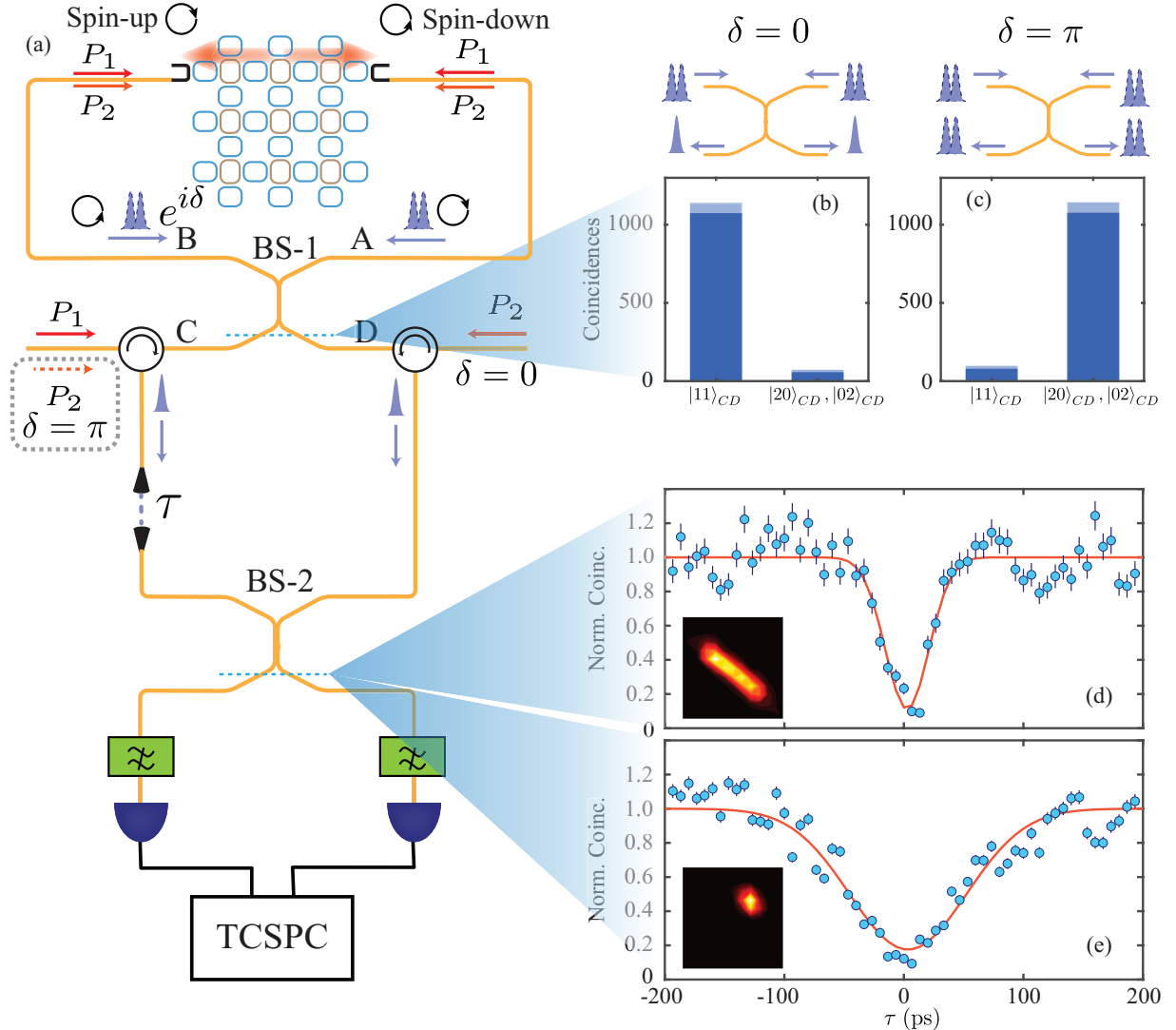


FIG. 3. (a) Schematic of the Sagnac interferometer setup used to deterministically split the two photons via time-reversed HOM interference of a path-entangled two-photon state (at beamsplitter BS1), and subsequently, realize HOM interference at beamsplitter BS2 with a variable delay  $\tau$  between the two photons. (b) Measured two-fold coincidences at the output ports C, D of the beam splitter BS1, for two different configurations so the input pump beams. The photons anti-bunch (bunch,  $\delta = \pi$ ) when the two pumps are in separate (same,  $\delta = 0$ ) input ports of BS1. (c,d) Measured HOM interference dip for  $\delta = \pi$ , and the pump frequencies  $(\delta\omega_{p_1}, \delta\omega_{p_2}) = (0, 0) J$ , and  $(0.8, 0.8) J$ , respectively. Insets show the measured JSI.

C and D of the beamsplitter BS-1. We pump our source in the middle of the edge band, that is,  $\delta\omega_{p_1} \simeq 0 \simeq \delta\omega_{p_2}$ . We introduce a relative delay between the two photons, interfere them on another beamsplitter (BS-2), and measure the coincidence counts at the output of BS-2 as a function of the delay  $\tau$  between the photons. As expected, we see a HOM dip in the coincidence counts, with a visibility of 88(10)%, which confirms that the two photons are indeed indistinguishable.

We note that the temporal width of the HOM interference dip is inversely related to the spectral width of the joint-spectral intensity (along the line  $\delta\omega_s = -\delta\omega_i$ ) that characterizes the two-photon state. As we demonstrated in Fig.2, we can control the JSI of generated photons in our source by simply tuning the input pump frequencies (Fig.2). To demon-

strate similar control in the HOM interference, we set the two pump frequencies to be at one of the extremes of the edge band  $\delta\omega_{p_1} \simeq 0.8 J \simeq \delta\omega_{p_2}$  such that the spectral width of the JSI is limited to  $\approx 0.8 J$  (Fig.2d). We now observe that the temporal width of the HOM interference dip is indeed much larger (by a factor of  $\approx 2.7(4)$ ) compared to the case with both the pumps in the center of the edge band. The discrepancy between this factor and the decrease in the spectral width (by a factor of 4.0(6)) can be accounted for by the limited spectral resolution of the JSI measurement.

Finally, we show that the generated two-photon state is energy-time entangled. The use of a continuous-wave pump for generating photon pairs via SFWM (or SPDC) naturally leads to the emergence of energy-time entanglement such that

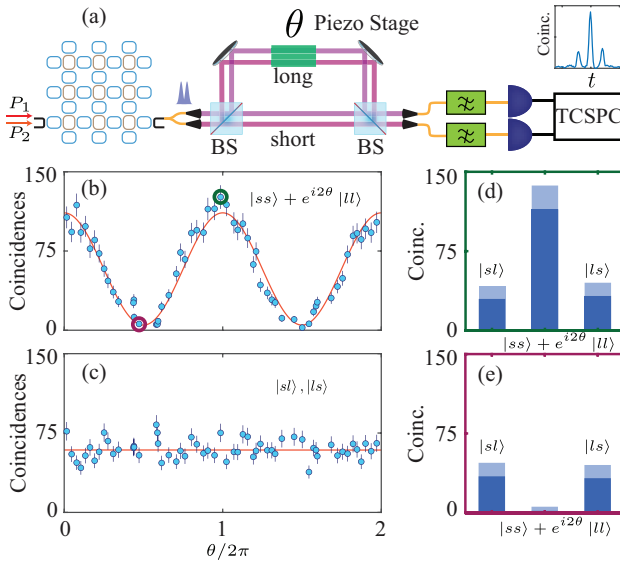


FIG. 4. (a) Schematic of the Franson interferometer setup to show the energy-time entanglement of generated photon pairs. The delay between the short and the long paths is  $\approx 800$ ps, much longer than the photon pulse widths. (b) Measured two-fold coincidences in the central peak, that is, when both the photons travel through the same path (short or long), as a function of the interferometer phase  $\theta$ . (c) Measured two-fold coincidences in the side peaks, that is, when the photons travel through different paths and are therefore, distinguishable. (d-e) Measured histograms at two points indicated in (b), showing the maximum and the minimum coincidence counts in the central peak. The counts in the side peaks are almost constant. The error bars are calculated assuming Poisson statistics. The input pump frequencies are  $\delta\omega_{p_1} \simeq 0.8J \simeq \delta\omega_{p_2}$  for this experiment.

$\Delta\omega\Delta T < 1$ , where  $\Delta\omega = \Delta(\omega_s + \omega_i)$  is the uncertainty in the total energy of the signal and idler photons, set by the pump bandwidth.  $\Delta T$  is the uncertainty in the time duration between arrival of two photons [37]. We use a beam splitter to probabilistically split the two photons at the output of our source, and inject them into two Franson interferometers with a path-length delay ( $\approx 800$  ps) much larger than the temporal correlation of the generated photons ( $\Delta T \approx 200$  ps, as shown in Fig.2(b)). Time-resolved coincidence measurements at the outputs of the interferometers show three peaks (Fig.4). The two side peaks correspond to the two cases when one of the photons took a shorter path in the interferometer, and the other took a longer path. The center peak corresponds to the two cases when both photons took either the shorter path ( $|ss\rangle$ ) or the longer path ( $|ll\rangle$ ). We measure the number of coincidence counts in the three peaks as we vary the phase  $\theta$  of the interferometers. The latter two cases (both short or both long) are indistinguishable, and therefore, we observe interference fringes in the coincidence counts as a function of the two-photon phase  $2\theta$  acquired in the interferometer. In contrast, the other two cases, where one photon travels through the shorter path and the other through the longer path ( $|sl\rangle, |ls\rangle$ ), are distinguishable and accordingly yield no interference. Our observation of two-photon interference fringes,

for a path-length delay that is much longer than the temporal correlation width  $\Delta T$  of the photons, demonstrates that the coherence time of the generated two-photon state ( $1/\Delta\omega$ ) is much longer than  $\Delta T$  and the two-photon state is indeed energy-time entangled.

As has been demonstrated earlier using a single-pump SFWM process in topological devices [31], the spectral correlations between the pump and the generated photon pairs are robust against fabrication disorders. We expect similar robustness for our dual-pump SFWM process as well. To show the robustness of spectral correlations of our source in the presence of disorder, we provide numerical simulation results in the supplementary information. We fix the input pump frequencies to be in the center of the edge band and calculate the spectra of generated photons for random realizations of disorder. We compare these results against those for a 1D array of ring resonators which is topologically trivial, and therefore, not expected to be robust against disorder. As expected, we observe that our topological source of indistinguishable photon pairs achieves much higher spectral similarity across devices when compared to a topologically trivial source.

In summary, we have demonstrated a topological source of indistinguishable photon pairs with tunable spectral-temporal correlations. Our demonstration could lead to on-chip generation of novel quantum states of light where topological phenomena are used for robust manipulations of the photonic mode structure and quantum correlations between photons. In particular, in the low-loss regime, our topological device can be used to generate single-mode squeezed light with a tunable spectrum, and at the same time, overcome the gain-bandwidth product that is inherent to single ring resonators. On a more fundamental level, nonlinear parametric processes such as four-wave mixing are inherently non-Hermitian in nature, that is, they do not conserve particle number. Therefore, our system paves the way for investigations of the rich interplay between topology, non-Hermitian physics, and quantum photonics processes to realize novel topological phases that are unique to photons.

This research was supported by the Air Force Office of Scientific Research Multidisciplinary University Research Initiative (AFOSR-MURI grant FA9550-16-1-0323) and the Physics Frontier Center at the Joint Quantum Institute. We thank Qudsia Quraishi for the nanowire detectors.

\* V.V.O. and S.M. contributed equally.

† Email: mittals@umd.edu

- [1] Braunstein, S. L. & van Loock, P. Quantum information with continuous variables. *Rev. Mod. Phys.* **77**, 513–577 (2005).
- [2] Pfister, O. Continuous-variable quantum computing in the quantum optical frequency comb. *Journal of Physics B: Atomic, Molecular and Optical Physics* **53**, 012001 (2019).
- [3] Hamilton, C. S. *et al.* Gaussian boson sampling. *Phys. Rev. Lett.* **119**, 170501 (2017).

[4] Vernon, Z. *et al.* Scalable squeezed-light source for continuous-variable quantum sampling. *Phys. Rev. Applied* **12**, 064024 (2019).

[5] Silverstone, J. W. *et al.* On-chip quantum interference between silicon photon-pair sources. *Nature Photonics* **8**, 104 (2014).

[6] He, J. *et al.* Ultracompact quantum splitter of degenerate photon pairs. *Optica* **2**, 779–782 (2015).

[7] Zhao, Y. *et al.* Near-degenerate quadrature-squeezed vacuum generation on a silicon-nitride chip. *Phys. Rev. Lett.* **124**, 193601 (2020).

[8] Zhang, Y. *et al.* Single-mode quadrature squeezing using dual-pump four-wave mixing in an integrated nanophotonic device (2020). 2001.09474.

[9] Dutt, A. *et al.* On-chip optical squeezing. *Phys. Rev. Applied* **3**, 044005 (2015).

[10] Takeda, S. & Furusawa, A. Toward large-scale fault-tolerant universal photonic quantum computing. *APL Photonics* **4**, 060902 (2019).

[11] Asavanant, W. *et al.* Generation of time-domain-multiplexed two-dimensional cluster state. *Science* **366**, 373–376 (2019).

[12] Larsen, M. V., Guo, X., Breum, C. R., Neergaard-Nielsen, J. S. & Andersen, U. L. Deterministic generation of a two-dimensional cluster state. *Science* **366**, 369–372 (2019).

[13] Lu, L., Joannopoulos, J. D. & Soljačić, M. Topological photonics. *Nature Photonics* **8**, 821 (2014).

[14] Khanikaev, A. B. & Shvets, G. Two-dimensional topological photonics. *Nature Photonics* **11**, 763–773 (2017).

[15] Ozawa, T. *et al.* Topological photonics. *Rev. Mod. Phys.* **91**, 015006 (2019).

[16] Haldane, F. D. M. & Raghu, S. Possible realization of directional optical waveguides in photonic crystals with broken time-reversal symmetry. *Phys. Rev. Lett.* **100**, 013904 (2008).

[17] Wang, Z., Chong, Y., Joannopoulos, J. D. & Soljačić, M. Observation of unidirectional backscattering-immune topological electromagnetic states. *Nature* **461**, 772–775 (2009).

[18] Hafezi, M., Demler, E. A., Lukin, M. D. & Taylor, J. M. Robust optical delay lines with topological protection. *Nature Physics* **7**, 907 (2011).

[19] Kraus, Y., Lahini, Y., Ringel, Z., Verbin, M. & Zilberberg, O. Topological States and Adiabatic Pumping in Quasicrystals. *Phys. Rev. Lett.* **109**, 106402 (2012).

[20] Hafezi, M., Mittal, S., Fan, J., Migdall, A. & Taylor, J. Imaging topological edge states in silicon photonics. *Nature Photonics* **7**, 1001 (2013).

[21] Rechtsman, M. C. *et al.* Photonic Floquet topological insulators. *Nature* **496**, 196–200 (2013).

[22] Mittal, S. *et al.* Topologically robust transport of photons in a synthetic gauge field. *Phys. Rev. Lett.* **113**, 087403 (2014).

[23] St-Jean, P. *et al.* Lasing in topological edge states of a one-dimensional lattice. *Nat. Photonics* **11**, 651–656 (2017).

[24] Bahari, B. *et al.* Nonreciprocal lasing in topological cavities of arbitrary geometries. *Science* **358**, 636–640 (2017).

[25] Bandres, M. A. *et al.* Topological insulator laser: Experiments. *Science* **359** (2018).

[26] Lu, L., Gao, H. & Wang, Z. Topological one-way fiber of second Chern number. *Nature Communications* **9**, 5384 (2018).

[27] Cheng, X. *et al.* Robust reconfigurable electromagnetic pathways within a photonic topological insulator. *Nature Mater.* **15**, 542–548 (2016).

[28] Zhao, H. *et al.* Non-hermitian topological light steering. *Science* **365**, 1163–1166 (2019).

[29] Barik, S. *et al.* A topological quantum optics interface. *Science* **359**, 666–668 (2018).

[30] Tambasco, J.-L. *et al.* Quantum interference of topological states of light. *Science Advances* **4** (2018).

[31] Mittal, S., Goldschmidt, E. A. & Hafezi, M. A topological source of quantum light. *Nature* **561**, 502 (2018).

[32] Blanco-Redondo, A., Bell, B., Oren, D., Eggleton, B. J. & Segev, M. Topological protection of biphoton states. *Science* **362**, 568–571 (2018).

[33] Haldane, F. D. M. Model for a quantum hall effect without landau levels: Condensed-matter realization of the “parity anomaly”. *Phys. Rev. Lett.* **61**, 2015 (1988).

[34] Leykam, D., Mittal, S., Hafezi, M. & Chong, Y. D. Reconfigurable topological phases in next-nearest-neighbor coupled resonator lattices. *Phys. Rev. Lett.* **121**, 023901 (2018).

[35] Mittal, S., Orre, V. V., Leykam, D., Chong, Y. D. & Hafezi, M. Photonic anomalous quantum hall effect. *Phys. Rev. Lett.* **123**, 043201 (2019).

[36] Chen, J., Lee, K. F. & Kumar, P. Deterministic quantum splitter based on time-reversed hong-ou-mandel interference. *Phys. Rev. A* **76**, 031804 (2007).

[37] Franson, J. D. Bell inequality for position and time. *Phys. Rev. Lett.* **62**, 2205–2208 (1989).

[38] Hong, C. K., Ou, Z. Y. & Mandel, L. Measurement of subpicosecond time intervals between two photons by interference. *Phys. Rev. Lett.* **59** (1987).

## Supplementary Information: Tunable quantum interference using a topological source of indistinguishable photon pairs

Venkata Vikram Orre,<sup>1,2,\*</sup> Sunil Mittal,<sup>1,2,†</sup> Elizabeth A. Goldschmidt,<sup>3</sup> and Mohammad Hafezi<sup>1,2,4</sup>

<sup>1</sup>*Joint Quantum Institute, NIST/University of Maryland, College Park, Maryland 20742, USA*

<sup>2</sup>*Department of Electrical and Computer Engineering and IREAP, University of Maryland, College Park, Maryland 20742, USA*

<sup>3</sup>*Department of Physics, University of Illinois at Urbana-Champaign, Urbana, Illinois 61801, USA*

<sup>4</sup>*Department of Physics, University of Maryland, College Park, MD 20742, USA*

### S1: CAR AND COINCIDENCES

In the main text, we characterized the intensity correlations between generated photon pairs by measuring the second-order cross correlation function  $g^{(2)}(\tau)$ . Here, we estimate the signal-to-noise ratio of our source by measuring coincidences to accidental ratio (CAR). We integrate  $g^{(2)}(\tau)$  around the peak to calculate the actual coincidences and divide it by the mean at  $\tau \gg 0$  which are the accidental coincidences. Our source achieves a CAR of  $\approx 53$  showing that the SNR is high. We also verify the behaviour of CAR as a function of one of the pump powers when the other pump is fixed. The CAR is expected to follow the equation

$$CAR = \frac{\eta P_{p_1} P_{p_2}}{(P_{p_1}^2 + P_{p_2}^2 + P_{p_1} P_{p_2})^2}, \quad (S1)$$

where the  $P_{p_i}$  is the power of the pump  $i$ . The CAR increases to a maximum and then decreases as a function of pump power. For low pump power, the CAR is limited by noise from the single-pump SFWM process. Fig. S1(b) shows the measured CAR as function of one pump power as the other pump power is fixed at 3 mW and agrees very well with the corresponding theoretical curve. We also verified that coincidences are from DP-SFWM by varying one of the pump powers, while the other is fixed at 3mW (Fig. S1(a)). As expected, we observe that the coincidence counts increase linearly as  $P_{p_1} P_{p_2}$ .

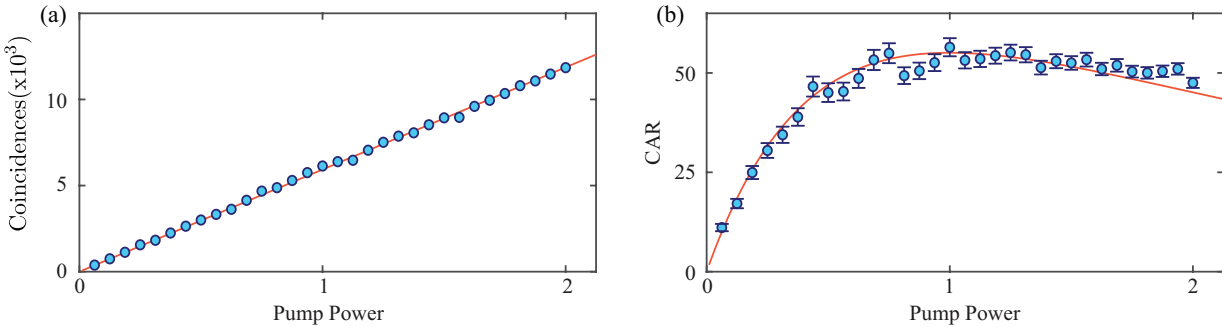


FIG. S1. (a) Coincidences, and (b) CAR as function of one of the pumps powers, while the other pump power is fixed at 3mW.

### S2: JSI IN THE BULK BAND

Figure S2 shows the measured the JSI of the signal and idler photons, when the input pump frequencies are in the bulk band of the device, that is, when  $(\delta\omega_{p_1}, \delta\omega_{p_2}) = (-2.42, -2.42) J$ , and  $(-1.82, -2.42) J$ . In contrast to the case where both the pumps are in the edge band, here we observe that the shape of the JSI changes significantly for different pump configurations. This is due to the fact that the bulk band does not have a well defined momentum and its dispersion is very sensitive to fabrication disorder.

### S3: FRANSON INTERFEROMETER SETUP

In figure 4 of the main text, we showed the two-photon coherence of generated photons using a Franson interferometer. The setup of Franson interferometer is implemented using Michelson configuration. The photon pairs generated from the chip were

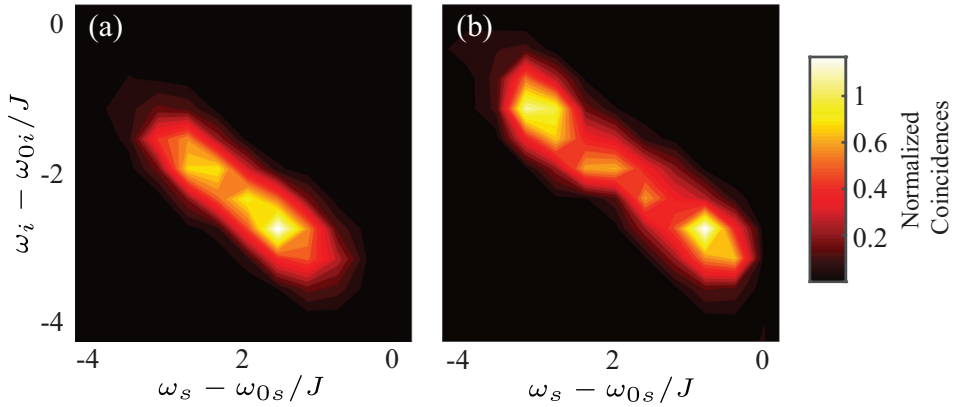


FIG. S2. Measured JSI when pumps are excited in the bulk band, (a)  $(\delta\omega_{p1}, \delta\omega_{p2}) = (-2.42, -2.42) J$ , (b)  $(\delta\omega_{p1}, \delta\omega_{p2}) = (-1.82, -2.42) J$

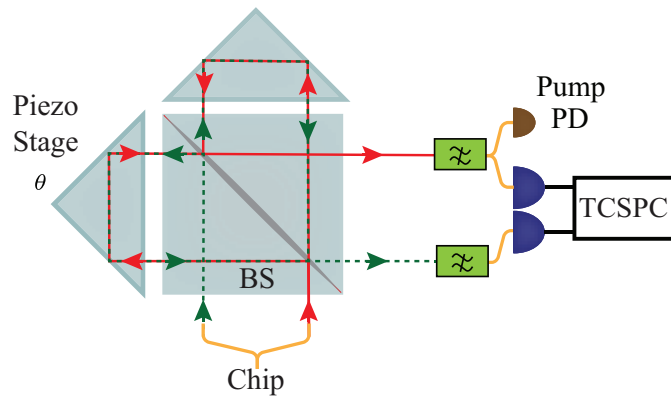


FIG. S3. Franson interferometer setup for two-photon coherence

split using a beam-splitter and coupled into two separate spatial modes of the same interferometer as shown in Fig. S3. The phase of the interferometer( $\theta$ ) shifts equally for both the spatial modes and is changed by a piezo-controlled delay stage. The two output beams from the interferometer are sent through filters and the coincidences are detected using TCSPC and SNSPDs.

#### S4: ROBUSTNESS OF SPECTRAL CORRELATIONS

To show the robustness of spectral correlations of our source in the presence of disorder, we perform numerical simulations to calculate the spectra of generated photons in the presence of random disorder. We introduce the disorder using random variations in the ring resonator frequencies, where the disorder strength is given by  $V$ . We fix the input pump frequencies  $(\omega_{p1}, \omega_{p2}) = (0, 0) J$ . We average over 100 random realizations for each disorder and calculate the mean similarity of the disordered spectra with the spectra in the absence of any disorder. We compare the results against those obtained for a topologically trivial 1D array of resonators. The 1D array consists of 10 ring resonators. As shown in Fig.S4, our topological source of indistinguishable photon pairs achieves much higher spectral similarity across devices when compared to a topologically trivial source. We also observe that the variability of 1D devices are much higher compared to 2D devices for larger disorders. These results show the robust nature of the edge states for photon generation.

The similarity between two devices  $i$  and  $j$  is calculated by taking the mean of the inner product between two spectra and is given by,

$$S_{i,j} = \frac{\sqrt{\int \Gamma_i \Gamma_j}}{\int \Gamma_i \int \Gamma_j}^2 \quad (S2)$$

where  $\Gamma_{i,j}$  is the spectra of generated photons for a device  $i,j$ .

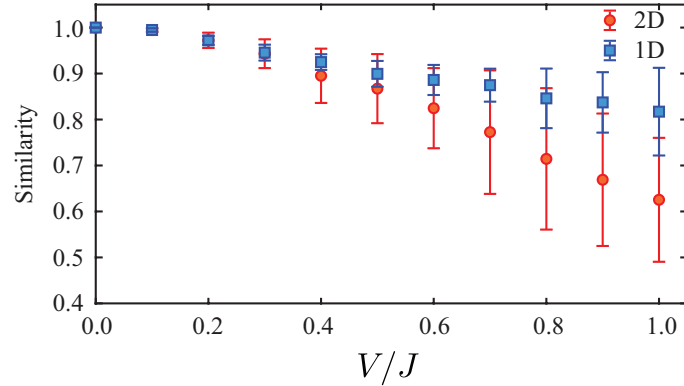


FIG. S4. Numerical simulation results for similarity in the spectra of generated photons as a function of disorder for 1D array and topological devices. 1D devices are much susceptible to disorder. The data is take for fixed input pump frequencies  $(\omega_{p1}, \omega_{p2}) = (0, 0)J$ .

\* V.V.O. and S.M. contributed equally.

† Email: mittals@umd.edu